Available online at www.sciencedirect.com
ScienceDirect
Icarus 193 (2008) 334–343
ICARUS
www.elsevier.com/locate/icarus

Hydrocarbons on Saturn's satellites Iapetus and Phoebe

Dale P. Cruikshank [a,*], Eric Wegryn [b], C.M. Dalle Ore [b], R.H. Brown [c], J.-P. Bibring [e], B.J. Buratti [d], R.N. Clark [f], T.B. McCord [g], P.D. Nicholson [h], Y.J. Pendleton [a], T.C. Owen [i], G. Filacchione [j], A. Coradini [j], P. Cerroni [j], F. Capaccioni [j], R. Jaumann [k], R.M. Nelson [d], K.H. Baines [d], C. Sotin [l], G. Bellucci [m], M. Combes [n], Y. Langevin [e], B. Sicardy [n], D.L. Matson [d], V. Formisano [j], P. Drossart [n], V. Mennella [o]

[a] *NASA Ames Research Center, Moffett Field, CA 94035, USA*
[b] *SETI Institute, 515 N. Whisman Road, Mountain View, CA 94043, USA*
[c] *Lunar and Planetary Laboratory and Steward Observatory, University of Arizona, Tucson, AZ 85721, USA*
[d] *Jet Propulsion Laboratory, 4800 Oak Grove Drive, Pasadena, CA 91109, USA*
[e] *Institut d'Astrophysique Spatiale, Université de Paris-Sud, Bâtiment 121, F-91405 Orsay, France*
[f] *US Geological Survey, Mail Stop 964, Box 25046, Denver Federal Center, Denver, CO 80225, USA*
[g] *Space Science Institute NW, 22 Fiddler's Road, Winthrop, WA 98862, USA*
[h] *Cornell University, 418 Space Sciences Building, Ithaca, NY 14853, USA*
[i] *Institute for Astronomy, University of Hawaii, 2680 Woodlawn Dr., Honolulu, HI 96822, USA*
[j] *INAF-IASF, Istituto di Astrofisica Spaziale e Fisica Cosmica, Via Fosso del Cavaliere 100, I-00133 Roma, Italy*
[k] *DLR, Institute for Planetary Exploration, Rutherfordstrasse 2, D-12489 Berlin, Germany*
[l] *University of Nantes, B.P. 92208, 2 rue de la Houssinière, 44072 Nantes Cedex 3, France*
[m] *INAF-IASF Istituto dello Spazio Interplanetario, Via del Fosso del Cavaliere 100, 00133 Roma, Italy*
[n] *Observatoire de Paris–Meudon, Département Recherche Spatial, 5 Place Jules Jannsen, 95129 Meudon Cedex, France*
[o] *INAF-OAC, Osservatorio Astronomico di Capodimonte, Salita Moiariello 16, I-80131 Napoli, Italy*

Received 7 October 2006; revised 19 March 2007

Available online 27 June 2007

Abstract

Material of low geometric albedo ($p_V \leqslant 0.1$) is found on many objects in the outer Solar System, but its distribution in the saturnian satellite system is of special interest because of its juxtaposition with high-albedo ice. In the absence of clear, diagnostic spectral features, the composition of this low-albedo (or "dark") material is generally inferred to be carbon-rich, but the form(s) of the carbon is unknown. Near-infrared spectra of the low-albedo hemisphere of Saturn's satellite Iapetus were obtained with the Visible–Infrared Mapping Spectrometer (VIMS) on the Cassini spacecraft at the fly-by of that satellite of 31 December 2004, yielding a maximum spatial resolution on the satellite's surface of ~65 km. The spectral region 3–3.6 μm reveals a broad absorption band, centered at 3.29 μm, and concentrated in a region comprising about 15% of the low-albedo surface area. This is identified as the C–H stretching mode vibration in polycyclic aromatic hydrocarbon (PAH) molecules. Two weaker bands attributed to $-CH_2-$ stretching modes in aliphatic hydrocarbons are found in association with the aromatic band. The bands most likely arise from aromatic and aliphatic units in complex macromolecular carbonaceous material with a kerogen- or coal-like structure, similar to that in carbonaceous meteorites. VIMS spectra of Phoebe, encountered by Cassini on 11 June 2004, also show the aromatic hydrocarbon band, although somewhat weaker than on Iapetus. The origin of the PAH molecular material on these two satellites is unknown, but PAHs are found in carbonaceous meteorites, cometary dust particles, circumstellar dust, and interstellar dust.

Keywords: Iapetus; Organic chemistry; Satellites, composition; Spectroscopy

* Corresponding author. Fax: +1 650 604 6779.
E-mail address: dale.p.cruikshank@nasa.gov (D.P. Cruikshank).

0019-1035/$ – see front matter
doi:10.1016/j.icarus.2007.04.036

1. Introduction

Saturn's third largest satellite, Iapetus (radius 720 km), has the unique property that the hemisphere centered on the apex of its locked synchronous orbital motion around Saturn has a very low surface reflectance (geometric albedo) of 2–6%, while the opposite hemisphere is about 10 times more reflective and has spectral absorption bands indicating that it is primarily composed of H_2O ice (e.g., Cruikshank et al., 1983). The nature and origin of the material on the "dark side" of Iapetus have been open questions since its discovery by inference (Cassini, 1962) and its verification three centuries later by observation (Murphy et al., 1972; Zellner, 1972).

Colorimetric and spectroscopic studies of the low-albedo material from ground-based telescopes have established that it is very red in color (strong positive slope of its spectral reflectance toward longer wavelengths). It also exhibits broad spectral features in the visible region (Vilas et al., 1996) that Gudipati et al. (2003) have examined in terms of broad emission features arising from the ultraviolet irradiation of aromatic hydrocarbons in the surface materials. The low-albedo material also has a very strong, broad absorption band at 3 μm (Owen et al., 2001). Modeling the entire spectrum from 0.4 to 4.1 μm with Hapke's scattering theory, Owen et al. (2001) found a satisfactory fit with a simple mixture of a nitrogen-rich tholin, amorphous carbon, and a small amount of H_2O ice. The importance of the tholin in the Owen et al. (2001) model is three-fold; it yields the notable red color, the very strong absorption band at 3 μm, and the rapid rise in reflectance at $\lambda > 3.2$ μm (in contrast to the 3 μm H_2O ice band) exhibited by the Iapetus low-albedo material.

At the flyby of Iapetus by the Cassini spacecraft at the end of December 2004, the Visible–Infrared Mapping Spectrometer (VIMS) obtained near-infrared spectral image cubes in which the low-albedo material is spatially resolved, permitting spectral mapping of the surface. Buratti et al. (2005) modeled the VIMS data from 0.9 to 5 μm with a mixture of the same nitrogen-rich tholin used by Owen et al. (2001), Fe_2O_3, H_2O ice, and a significant quantity of HCN polymer, finding an approximate fit to the overall shape of the spectrum and to the strong 3-μm band. A prominent absorption band at 2.41 μm remains unidentified, although Clark et al. (2005a, 2005b) have proposed a cyanide compound identification. Buratti et al. (2005) also found carbon dioxide on the low-albedo side; its spectral band is slightly shifted from the normal wavelength of pure CO_2, suggesting that this molecule is in some way complexed with another component, perhaps the H_2O ice (Chaban et al., 2007). A broad, weak absorption band centered near 1.0 μm found in the VIMS data has been interpreted as ferric iron (e.g., Fe_2O_3) (Buratti et al., 2005).

More distant from Saturn, Phoebe is presumed to be a captured satellite because of its inclined, elliptical retrograde orbit. It is irregular in shape, with approximate dimensions 115×105 km (radii). Its low albedo and the presence of H_2O ice were known from ground-based observations (e.g., Owen et al., 1999). Clark et al. (2005a, 2005b) reported the first Cassini VIMS observations from the close approach of Phoebe in June 2004, as the spacecraft approached Saturn for orbital insertion. VIMS spectra revealed, in addition to H_2O ice, ferrous–iron bearing minerals, bound water, trapped CO_2, probable phyllosilicates, and absorption band bands attributed to organics, nitriles, and cyanide compounds.

In this paper we report the detection of hydrocarbon absorption bands in the material of the low-albedo hemisphere of Iapetus and a further elaboration of those reported by Clark et al. (2005a, 2005b) on Phoebe. These bands, which are similar to those seen in the spectra of interstellar diffuse clouds, indicate the presence of both aromatic and aliphatic hydrocarbons. The aromatic hydrocarbon band on Phoebe is significantly weaker than on Iapetus, as discussed below.

2. The data

2.1. Iapetus

The VIMS instrument is described by Brown et al. (2004), and a description of some of the first observations in the Saturn system is found in Brown et al. (2006). The observations analyzed here were taken during the flyby of 31 December 2004, and represent the closest approach and the highest quality, spatially resolved, spectra of Iapetus ever obtained. Four sets of images and VIMS spectral cubes were taken at roughly 4-h intervals at the time of the close flyby of 2004 December 31. The spacecraft was near the apoapsis in its highly elliptical orbit when it approached within 130,000 km of Iapetus, meaning that the spacecraft was moving relatively slowly, while Iapetus flew past rapidly. The result was a relatively small change in subspacecraft point from mosaic to mosaic, but a large change in illuminated phase, from gibbous to crescent, as Iapetus passed Cassini. The spacecraft had a view of roughly three quarters of the illuminated leading hemisphere as the satellite approached. The view decreased to less than half of the disk as the satellite passed the spacecraft. At closest approach, VIMS achieved a resolution of about 20 spatial pixels across the 1436 km diameter satellite, corresponding to a maximum resolution (at center of disk) of ∼65 km per pixel. The VIMS datasets relevant to this study are listed in Table 1.

2.2. Phoebe

The Cassini spacecraft flew by Phoebe on its way to Saturn orbital insertion around the planet, and made its closest approach on 11 June 2004. High-resolution images of some regions of the object were obtained with spatial resolution ∼20 m, while the resolution exceeded 2 km/pixel for most of the surface (Porco et al., 2005). VIMS obtained observations throughout the encounter, and those data have been analyzed and described by Clark et al. (2005a, 2005b). VIMS data were taken from 08:47 UT at an initial range of 245,833 km and phase angle 84.9° on 11 June 2004, to 10:22 UT on 12 June, at a final range of 338,401 km and phase angle 92.2°. The closest image was obtained at 19:32 UT on 11 June, at a range of 2178 km and phase angle 24.6°. Much of the surface was covered with spatial resolution 1 km/pixel (Clark et al., 2005a, 2005b). Here

Table 1
Parameters of the VIMS datasets for Iapetus and Phoebe

Dataset Iapetus	31 Dec. 2004 (UTC)	Phase angle (deg)	VIMS cubes used in this work	Range (km)	Sub-spacecraft point
COMPA001	03:34		CM_1483156810		33 N, 69 W
LIMBTOPOB	08:17	63	CM_1483172847	*146,500*	45 N, 64 W
			CM_1483174086		
GLOBMAPC	14:04	79	CM_1483194809	*128,500*	55 N, 48 W
			CM_1483195512		
LIMBTOPOD	18:30	93	CM_1483210589	*126,500*	67 N, 26 W
LIMBTOPOE	22:10	105	CM_1483224541	*124,500*	85 N, 30 W
Dataset Phoebe	11 June 2004 (UTC)		VIMS cubes	Range (km)	Sub-spacecraft point
PHOEBE017	19:22		CM_1465674369	4800	
			CM_1465674563	3500	

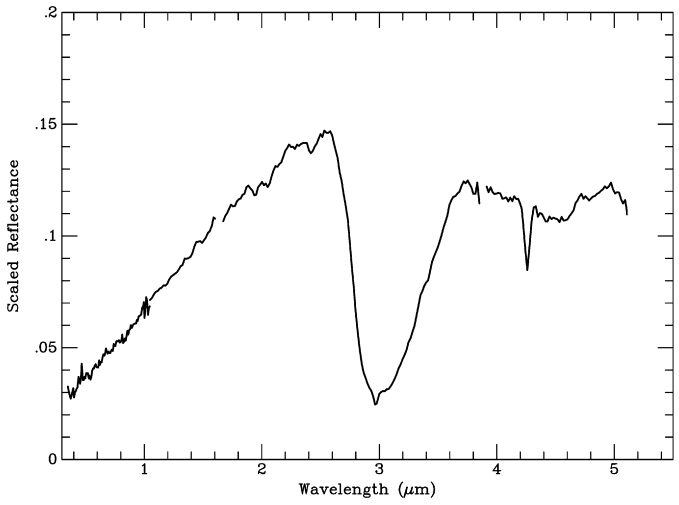

Fig. 1. This shows the grand average of all pixels on the low-albedo material on Iapetus, from all the VIMS cubes listed in Table 1 and additional data cubes not presented here. Reflectance is scaled to 0.14 at 2.2 μm to be consistent with the geometric albedo at that wavelength as observed from Earth at small phase angles (Owen et al., 2001). Modified from Brown et al. (2006).

we examine the spectrum of Phoebe representing the average of all the spatial pixels contained in two closest approach cubes noted in Table 1. We discuss the result of our investigation of the data in Section 3.2.

3. Data analysis

3.1. Iapetus

The grand, or overall average spectrum of the low-albedo material on Iapetus (Fig. 1), consisting of 3226 spatial pixels, shows the basic spectral characteristics at high signal precision (Brown et al., 2006). The deep, broad absorption band centered at 3 μm on Iapetus is attributed to a combination of N–H in the nitrogen-rich tholins used to model the spectrum (Owen et al., 2001; Buratti et al., 2005), and O–H in the small amount of H_2O ice that may occur as a thin coating on or within the dark material. The weakness of the 1.5 and 2.0-μm H_2O ice bands, as well as the steep rise in reflectance beyond 3.2 μm, indicates a reduced abundance of H_2O on the surface of the low-albedo hemisphere of the satellite. In the present paper, we focus on inflections in the long-wavelength slope of the 3-μm band because this is where the diagnostic C–H stretching mode absorption bands of hydrocarbons accessible in the VIMS wavelength region occur.

An initial inspection of the spectrum in Fig. 1 suggested that there is some subtle structure in the region of the absorption bands of polycyclic aromatic hydrocarbons (PAH) at 3.29 μm, and aliphatic hydrocarbons near 3.4 μm (Brown et al., 2006). We therefore searched all of the high quality data from the five observations listed in Table 1 for absorption at the wavelength region of the C–H stretching mode in the aromatic hydrocarbons in the low-albedo material.

We used a standard algorithm to establish criteria for the selection of spatial pixels in the VIMS cubes that show an absorption band coincident with the C–H stretching mode band in PAHs. A continuum curve was defined using a spline fit to the upward sloping region of the spectrum beyond ∼3.2 μm, and the feature was identified by integrating the area under the continuum curve between 3.25 and 3.35 μm. The program flagged the pixels with the largest absorption over the six-channel interval between these two wavelengths (spectral bands 240 [3.248 μm] through 246 [3.350 μm]). Regions in or bordering on the high albedo region, which shows a strong absorption at 3 μm due to H_2O ice, were not included because the PAH feature sits on the lower right corner of this deep band, making detection problematic if not impossible. The flagged pixels were then validated by visual inspection to reject spurious detections due to spikes in the data.

The pixels selected for analysis here do not include all of the pixels in these datasets that showed a feature at the wavelength of interest. Rather, the pixels were selected based not only on the presence of a feature in the spectrum, but also for temporal continuity and spatial coherence. That is, geographical regions were defined (within the constraints of the rough spatial resolution of these VIMS cubes) that showed the PAH feature in numerous (if not all) contiguous pixels; these regions were also selected because they showed the PAH feature in roughly the same location in multiple mosaics, moving with the rotation of the satellite relative to the spacecraft. Other pixels that showed a feature in relative spatial isolation, or that showed a feature which did not reappear in the same location in other mosaics, were excluded. We note that the PAH absorption feature may be seen in other areas on Iapetus, and we estimate the areal coverage to be between 5 and 10% of the area of the low-albedo hemisphere.

A VIMS cube from the sequence COMPA001, taken on approach to Iapetus and at small phase angle, included the entire disk of the satellite. The search of this cube yielded 21 spatial pixels meeting the established criteria noted above. Data taken closer to Iapetus at larger and rapidly increasing phase angles did not generally include the whole satellite in a single field of view, but yielded temporally consecutive cubes taken at different spacecraft pointing directions to make mosaics of spatial pixels covering the entire satellite. A positive signal de-

fined by the criterion noted above was found in the first of these mosaics (LIMBTOPOB) in 33 pixels from a full frame, plus 31 pixels from one covering the lower (southern) portion of the disk. Analysis of this same region in the second mosaic (GLOBMAPC) yielded 14 and 19 pixels in two overlapping cubes with a strong detection. The third mosaic (LIMBTOPOD) showed only about 12 pixels with the feature, while in the fourth (LIMBTOPOE) the region was on the limb as Iapetus moved past the spacecraft; no pixels were selected from LIMBTOPOE, but we include it in Table 1 for completeness. In all, 130 spatial pixels were selected on the basis of the established criterion for averaging and for further study. The total number of spatial pixels included in the six cubes used in this study is ∼750, and those selected for this study amount to ∼17% of these pixels.

In Fig. 2 we present the average spectrum derived from each individual data cube, as noted in the previous paragraph. The spectra have been normalized and offset for clarity. The grand average of all 130 selected pixels from the six data cubes is also shown.

Fig. 3 shows the average spectrum of the 130 selected pixels, plus the global average of the low-albedo material (3226 pixels) derived from the full set of data from the 31 December 2004 encounter.

Numerous pixels in the four datasets show the absorption feature variously scattered in single pixels, and thus are not able to be precisely pinpointed spatially. However, one region of significant extent was discovered showing the PAH absorption feature prominently spread across a large area of Iapetus. The region lies at a northern latitude near the equator, roughly 0° to 30°, and longitude from about 30° to 120°. It includes a contiguous swath 2 to 3 pixels (up to 200 km) wide and 8 to 14 pixels (500 to 1000 km) long extending east-northeast from the center of the low-albedo hemisphere. There are also smaller clusters of pixels in and southwest of the large basin on the terminator. The main region of PAH concentration was best imaged in the first mosaic, and thereafter slowly rotated away from the spacecraft in subsequent mosaics, becoming nearly indistinguishable on the limb of the crescent satellite in the final dataset.

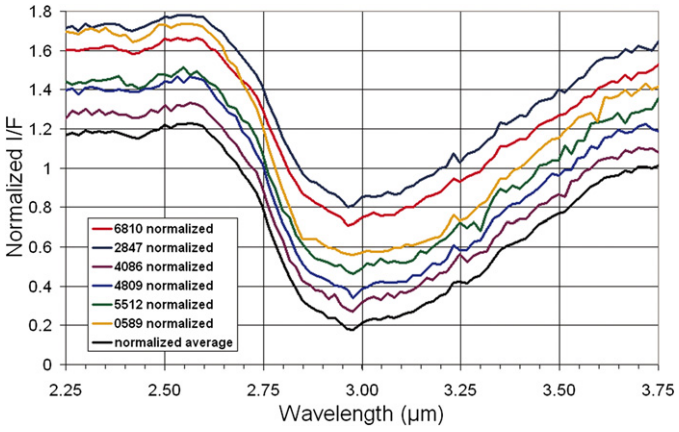

Fig. 2. Spectra of the selected pixels in each of the six VIMS image cubes, all normalized to 1.0 at 3.73 μm and offset vertically by multiples of 0.1, and the average (heavier black line) representing the total of 130 spatial pixels. The cube designations are from Table 1. The PAH absorption band lies between 3.25 and 3.35 μm.

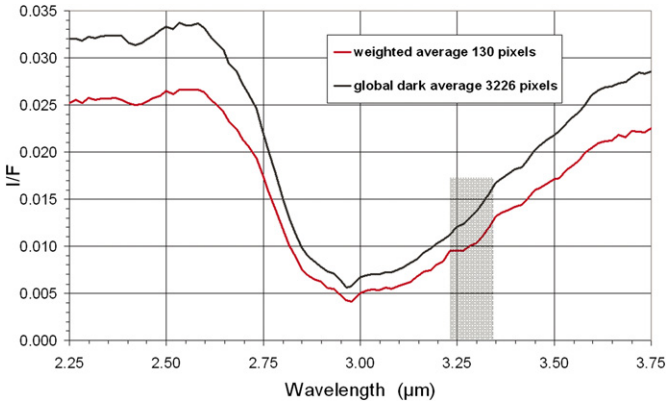

Fig. 3. Comparison of the global average of the low-albedo material and the weighted average of 130 pixels (from six VIMS cubes) selected for the PAH band at 3.29 μm. Shaded box shows the wavelength interval over which the algorithm searched for the band.

Although the spectral feature of interest is superimposed upon the slope of the very broad and deep absorption band centered at 3.0 μm, we proceeded to determine the profile of the 3.29-μm band with the assumption that the strengths of two superimposed absorption bands are largely additive. This assumption is valid in the case of scattering of sunlight from moderate albedo surfaces such as that of Pluto (e.g., Douté et al., 1999), where, for example, the narrow bands of solid N_2 and CO can be seen distinctly against the broader coincident absorption by solid CH_4 in the region ∼2.10–2.45 μm. Similarly, on the higher-albedo surface of Triton, narrow bands of solid N_2, CO, and CO_2 can be clearly seen against background absorption by solid H_2O and CH_4 (Quirico et al., 1999; Cruikshank et al., 2000). Modeling of the spectra of icy bodies by radiative transfer calculations generally confirms the additive behavior of coincident bands on these two objects. Among materials of low albedo, the same basic principle applies, such that in near-infrared diffuse reflectance spectra of carbonaceous meteorites the weak aliphatic C–H stretching mode absorption bands can be seen against the background broad absorption of structural O–H in the meteorite (e.g., Gaffey et al., 1993).

To determine the strengths of two or more superimposed absorption bands with high precision requires a deconvolution of the bands based on laboratory or computational data. We have not taken this step because of the uncertainty in modeling the strong band on Iapetus (and Phoebe), which itself arises from the overlap of O–H and N–H modes in the solid material of the surface (for the Iapetus case see Owen et al., 2001). Thus, our determinations of the strengths of the 3.29-μm bands in the spectra of Iapetus and Phoebe are to be taken as lower limits; the actual strength may be significantly greater.

We used two different spline fits at several points to the steeply sloped spectrum in order to extract the region of the absorption bands, thereby removing the local continuum. In this procedure we assumed that the steep slope is introduced entirely by the strong band attributed to N–H and O–H, as noted above. The splines were selected to represent different interpre-

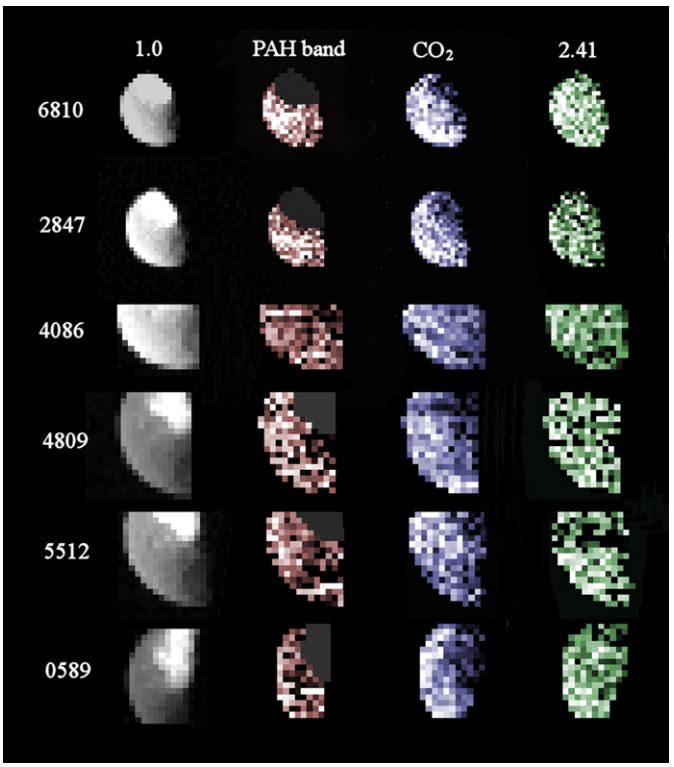

Fig. 4. Pixel maps from the six VIMS cubes of Iapetus used in this study. The numbers to the left of each row are the last four digits of the cube identifications given in Table 1. The left-hand column of images shows the VIMS view at 1.0 μm. The second column (PAH band) shows the strength of the PAH band at 3.29 μm (brighter pixels denote stronger absorption in the band as defined in the text). In some images in this column, the region of the bright polar H_2O ice has been masked. The third column shows the distribution of the CO_2 band at 4.26 μm, and the fourth column shows the distribution of the 2.41-μm band.

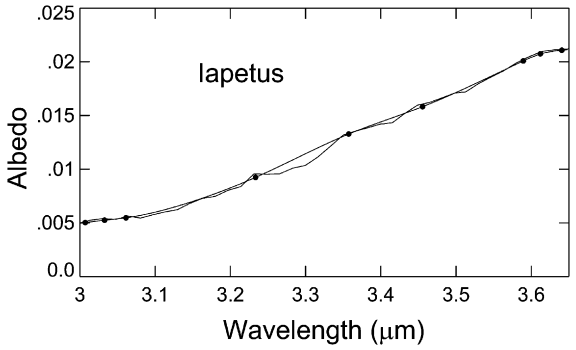

Fig. 5. Spline fit across the region of interest for the average of 130 points.

tations of the noise level in the spectrum; the spline that touches only the peaks in the spectrum represents the assumption that everything under the curve is a genuine absorption, while the spline that cuts through the mid-points of the 3.29-μm depression represents the most conservative interpretation. In either case, the absorption features at 3.29, 3.42, and 3.51 persist. We performed this process for each of the data sets in Table 1, and then for the grand average of 130 spatial pixels, as shown in Fig. 5.

The ratio of the Iapetus data to the best-fitting spline is shown in the upper trace of Fig. 6, together with a comparison

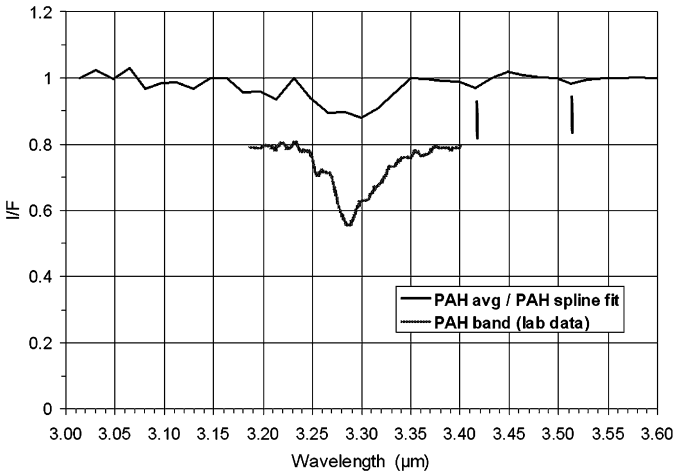

Fig. 6. Ratio of Iapetus PAH spectrum (130 pixel average) to the spline shown in Fig. 5. Offset below the Iapetus spectrum is a laboratory spectrum of the average of six different PAH molecules included for comparison (Colangeli et al., 1992). The two vertical lines indicate the positions of the $–CH_2–$ aliphatic stretching mode absorption bands.

spectrum of a mixture of six relatively small PAH molecules (primarily pentacene and benzo[α]pyrene) from the laboratory (Colangeli et al., 1992). In the Colangeli et al. (1992) spectra, the band central wavelength is the same in all components, though small differences in the band profiles occur. The coincidence in band width and central wavelength is evidence of the correct identification of the Iapetus band with PAH molecules. We note, however, that the coincidence of the band positions does not imply that the PAH molecules in the spectra of Iapetus and Phoebe are small, because band position is not directly dependent on molecular size.

After selecting the spatial pixels that show the 3.29-μm spectral feature in each of the four mosaics, we evaluated the noise in the spectrum across the full spectral range of the infrared channel of VIMS (∼1.0–5.1 μm) in the average of those selected pixels by removing the continuum using a noiseless spline across the spectrum in four wavelength increments. The spectrum was then ratioed to the spline in each segment and the errors calculated. This noise analysis is shown in Fig. 7 for the composite spectrum of the 130 selected pixels.

When ratioed with the continuum spline fit from only the 130 selected pixels the absorption band is distinctly visible. The depth of the 3.29 μm band in this normalized ratio plot (Fig. 6) is ∼0.11, and the uncertainty (1σ) from the plot in Fig. 7 is 0.018. This represents a 6-σ detection.

As noted, the search algorithm highlighted a subset of spatial pixels on Iapetus that showed a band centered at 3.29 μm. The same spectra show weak and narrower absorption peaks at 3.42 and 3.52 μm, which are coincident or very close to the $–CH_2–$ (methylene) wavelengths (3.42 and 3.51 μm) arising from the symmetric and asymmetric stretch of the $–CH_2–$ group in aliphatic hydrocarbons. Using the same noise analysis noted above for the PAH band, we estimate that the detections of the 3.42 and 3.52 μm bands are at approximately the 1.5- to 2-σ level. The $–CH_3$ (methyl) stretching bands in aliphatic hydrocarbons also occur in this wavelength region. In the inter-

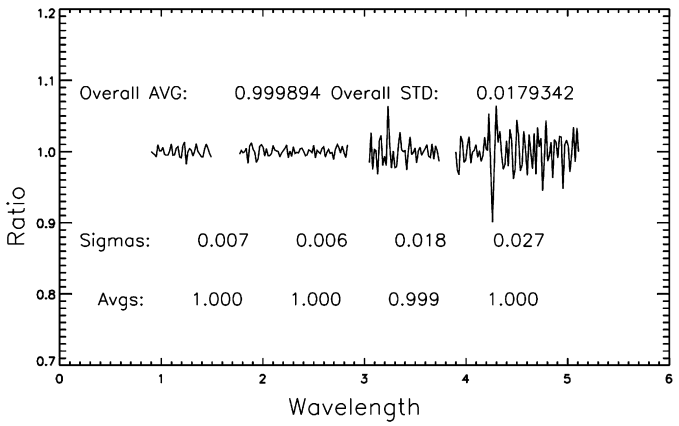

Fig. 7. Iapetus spectrum noise analysis for the 130-pixel composite spectrum shown in Figs. 4 and 5. The standard deviation across the region of the organic absorption bands is 0.018.

stellar medium (e.g., Pendleton and Allamandola, 2002, Figs. 5 and 8) the four bands of $–CH_2–$ and $–CH_3$ together occur in a cluster between 3.35 and 3.52 μm; in the laboratory the wavelengths of these bands are variable (±∼0.01 μm) depending on the molecule(s) in which they occur (Sandford et al., 1991; Pendleton et al., 1994), and the degree to which they may be ionized, dehydrogenated, or electronically excited (Jourdain de Muizon et al., 1986). These aliphatic stretching mode bands can appear in purely aromatic molecules when the presence of extra peripheral hydrogen atoms in H*n*-PAHS converts some of the peripheral aromatic carbons (–C–H) into aliphatic carbons ($–CH_2–$ groups) (Bernstein et al., 1996, 2005). Polycyclic aromatic hydrocarbons with associated C–H side groups are found in carbonaceous meteorites (Cronin et al., 1988), and in interstellar dust emission regions (Bernstein et al., 1996).

In complex macromolecular carbonaceous materials (e.g., kerogens, coals, bitumens), which is a probable representation of the material present on Iapetus, the bands in the 3.4- to 3.5-μm region do not show a clear correlation with $–CH_2$ and $–CH_3$ abundances.

Asymmetric vibrations of $–CH_3$ groups directly attached to aromatic rings can overlap the $–CH_2$ bands, and their separate identification can only be accomplished with high quality data in which the signal precision and band strength exceed those in the data for Iapetus (and Phoebe). We cannot, therefore, establish the identification of $–CH_2$ or $–CH_3$ from our data, although the data are certainly consistent with an aliphatic fraction including these two functional groups in some proportions.

Combination bands of the stretching and bending modes in $–CH_2–$ and $–CH_3$ occur in the region ∼2.27–2.31 μm (e.g., Moroz et al., 1998), but these are much weaker than the fundamentals and are not seen in the Iapetus spectrum. Additional, even weaker overtones and combinations of the stretching modes occur in the region ∼1.69–1.76 μm and are not seen in the Iapetus data. The combination aromatic C–H stretch and C=C stretch at 2.15–2.17 μm (Moroz et al., 1998, Table III) is consistent with a weak feature in the spectrum of Iapetus' dark material.

3.2. Quantitative estimate of the abundance of PAHs in the Iapetus surface material

As pointed out by several authors, including Bernstein et al. (2005), the wavelength region of the C–H stretching bands in PAH mixtures is not diagnostic of specific molecular species or molecular size, but only classes of species. However, because the stretching modes of all of the aromatic and aliphatic CH-bearing molecules overlap, under certain simplifying assumptions, a measurement of the bands gives a rough indication of the total abundance of these hydrocarbons in the sampled surface layer.

Using information about the intrinsic strength of the C–H stretch bands in PAHs, as determined in the laboratory and the strength of the band in the Iapetus spectrum, we can make an estimate of the abundance of these molecules in the layer of low-albedo material exposed to space on the surface of Iapetus. From laboratory spectroscopy of isolated molecules of different sizes, the intrinsic strength (integrated absorbance over the band width) per molecule, or A-value (in cm/molecule) has been determined for a number of PAHs (d'Hendecourt and Allamandola, 1986), with the result that $A \approx 2.6 \times 10^{18}$ cm/molecule.[1]

Following d'Hendecourt and Allamandola (1986), the column density (N) of absorbers in the band is $N = Cl$, where C is the concentration of absorbers (molecules/cm^3) and l is the pathlength through the material. With certain assumptions about the band shape (symmetrical, and near-Lorentzian), N can be approximated as

$$N \approx \tau \Delta\nu / A,$$

where τ is the optical thickness and $\Delta\nu$ is the width of the band.

The width (FWHM) of the 3.3-μm band on Iapetus (Fig. 7) is $\Delta\nu \sim 70$ cm^{-1}. For an estimated τ in the range 0.01 to 0.1, $N = 3 \times 10^{-19}$ to 3×10^{-18} C–H/cm^2. This is a lower limit because of the points raised above in the discussion of continuum definition and its effect on the absolute band strength in the Iapetus data. If the density of the material is 1 g/cm^3, the optical penetration depth of incident sunlight that is then scattered to the observer is ∼100 μm, and if these are small molecules with molecular weight ∼300 Da (mean molar mass 300 g/mole), we calculate a range of 10^{-4} to 10^{-3} g/cm^3 of aromatic molecules in the surface layer. The concentration is dependent on the penetration depth of the incident sunlight, and our choice of 100 μm penetration depth is only an estimate; actual penetration may be substantially less. If, however, the PAH absorption arises in kerogen- or coal-like macromolecular material, the overall abundance in the surface material may be much greater than noted above, and such material may constitute all or nearly all of the low-albedo surface component. See further discussion below.

[1] This value for A is the average of laboratory values for the following four relatively small molecules: $C_{10}H_8$, $C_{14}H_{10}$, $C_{48}H_{20}$, $C_{24}H_{12}$ (Allamandola and Mattioda, personal communication). For the calculation of the concentration of molecular material in the surface layer we use a mean molar mass of 300 g/mole.

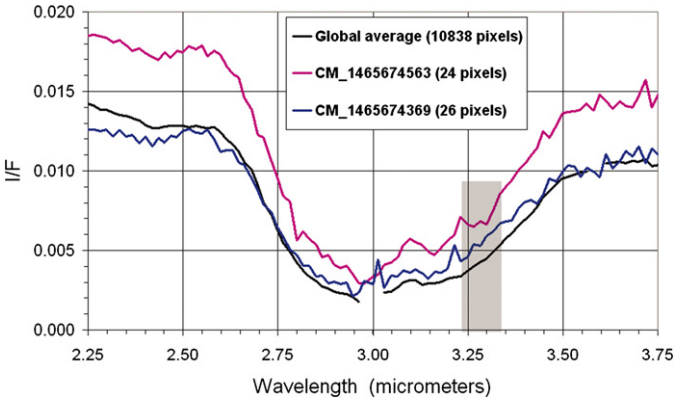

Fig. 8. Phoebe spectrum (heavy solid line), showing the global average of 10838 pixels derived from all favorable VIMS cubes (adapted from Clark et al., 2005a, 2005b). The other two traces show the average of 24 and 26 pixels from the cubes noted in the key and in Table 1. Shaded box shows the wavelength interval over which the algorithm searched for the band.

3.3. Phoebe

In their study of the VIMS data acquired during the encounter with Phoebe on 11 June 2004, Clark et al. (2005a, 2005b) noted that some regions of Phoebe show weak absorption bands around 3.3 μm indicating the presence of polycyclic or cycloalkane molecules in the surface materials. Phoebe's rich spectrum also reveals Fe^{2+}-bearing minerals, bound water, trapped CO_2, and probable phyllosilicates, nitriles, and cyanide compounds. For the present work we applied our search algorithm to the Phoebe data to extract those spatial pixels in which an absorption centered at 3.3 μm occurs. Coradini et al. (2006) have analyzed the Phoebe data from VIMS using a statistical technique designed to identify surface units that bear similar characteristics of reflectance level, band strength, and other parameters. Averaging the spectra from each of the identified groups having homogeneous characteristics improves the quality of the data, particularly in the longer wavelength regions ($\lambda > 3$ μm) where the signal is weak and noisy. From these improved spectra, Coradini et al. (2006) generally concur with Clark et al. (2005a, 2005b) in the identification of absorption bands that indicate the presence of silicates, organic molecules, nitriles, and cyanide compounds, and also reveal a few bands in addition to those found by Clark et al. (2005a, 2005b).

For the present paper, we conducted an analysis similar to that described above for Iapetus. As with Iapetus, the aromatic hydrocarbon absorption feature is seen in various single pixels in many of the numerous long- and mid-range VIMS cubes, but without the spatial resolution necessary to pinpoint their location on Phoebe. Yet analysis of the spectral cubes acquired during closest approach did reveal two well-defined patches on the surface of the irregularly shaped satellite. In general, the feature is less prominent and more widely scattered on Phoebe than on Iapetus.

Fig. 8 shows the spectra of two regions from the Phoebe closest approach mosaic (cubes CM_1465674563 and CM_1465674369), along with the global average spectrum of Phoebe for comparison. As with Iapetus, the PAH feature in these most concentrated patches shows an absorption on the order of 10% down from the adjacent continuum. It appears to have the same shape as the feature on Iapetus, and if there is any difference in wavelength it is perhaps shifted to slightly shorter wavelengths. The non-sphericity of Phoebe makes it challenging to identify well-defined regions with specific latitudes and longitudes in the longer range images.

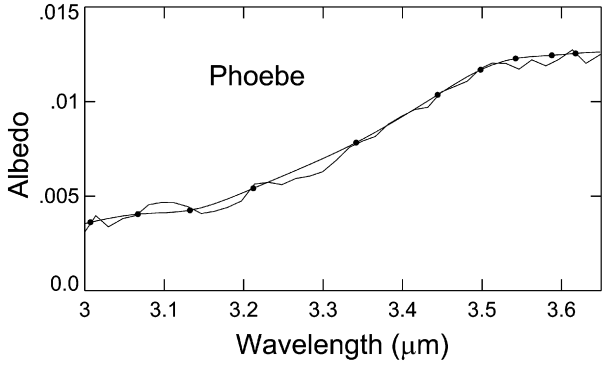

Fig. 9. Spline used to define the 3.29 μm PAH band on Phoebe.

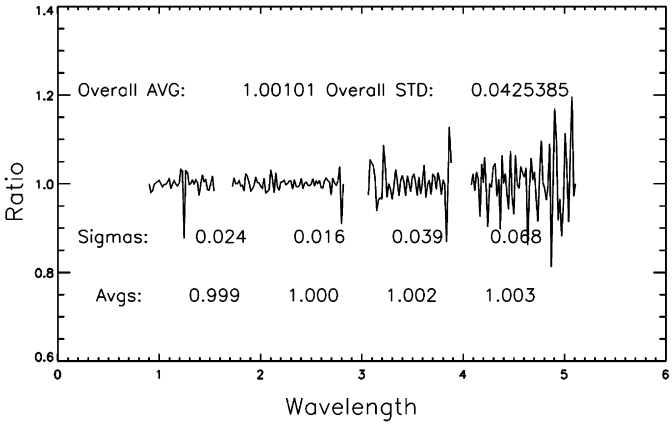

Fig. 10. Noise analysis for Phoebe spectrum. The standard deviation across the region of the organic absorption bands is 0.039.

The average of all 50 pixels from the two Phoebe cubes was fit with a spline (Fig. 9) to delineate the PAH band. A noise analysis of the same data set (Fig. 10) shows that the standard deviation across the spectral region of interest is 0.039, or about twice the value for the Iapetus noise level (Fig. 7).

3.3.1. PAH abundance on Phoebe

The PAH band on Phoebe is weaker than that on Iapetus, but it is clearly detectable in some regions of the satellite's surface. Because of the inherent large uncertainties in deriving an abundance of PAH molecules in an essentially opaque, scattering surface, we note here only that the band strength on Phoebe is less than on the regions of Iapetus where we found it to be concentrated.

4. Context in terms of organics in the Solar System

In view of the great uncertainty in the abundance of PAH-bearing material in the surface materials of Iapetus and Phoebe, we can only speculate on other materials (aside from H_2O ice,

which appears in the dark material of both bodies (Buratti et al., 2005; Clark et al., 2005a, 2005b). Buratti et al. (2005) fit the VIMS spectrum using tholins, generally consistent with the approach of Owen et al. (2001) in their study of ground-based data. Because tholins consist of macromolecular carbonaceous material of which PAH molecules and their aliphatic appendages are components (e.g., Imanaka et al., 2004; Bernard et al., 2006), the previous studies are generally in accord with the new spectral bands reported here. Besides tholins, other materials of low-albedo and weak spectral bands include certain minerals, elemental carbon and more complex kerogen-like molecular masses. Some opaque minerals of low albedo have no diagnostic spectral bands, but when present, have a significant effect on the reflectance of the surface material in which they are mixed. Elemental carbon is a logical possibility because it can arise from the dehydrogenation of aromatic and aliphatic molecules. Such carbon can be amorphous or can have varying degrees of graphitic structure. Graphitic structure can be produced directly by the dehydrogenation of large aromatic molecular networks if the dehydrogenating force is insufficient to break all of the hexagonal ring structures intrinsic to the aromatic progenitor materials. Graphitic structures with dimensions 3–4 nm are found in the nanocrystalline C cores of grains of circumstellar origin (extracted from carbonaceous meteorites). These are single planar sheets of sp^2 bonded carbon (an aromatic structure) and are called graphene. This material may represent a component in a structural continuum, with PAHs constituting the small size limit. Bernatowicz et al. (1996) found graphene and PAH-like material consisting of aromatic units less than 1 nm in size in the circumstellar grain cores, and suggest that both components were produced in the gas phase. Condensed PAHs may have provided the nuclei for further graphite growth from the cooling gas.

We do not know if the PAHs and the other refractory material of low albedo on Iapetus are of circumstellar origin, but we note that Messenger et al. (1998) found PAH concentrations up to 5 parts per thousand in individual circumstellar graphite grains extracted from two primitive meteorites, thus exceeding our estimated concentration of ∼1 part per thousand in the PAH-rich regions of Iapetus. This fact alone does not establish a connection to presolar material, but allows for the possibility that the organic molecules on Iapetus (and Phoebe) predate the formation of the Solar System.

Complex kerogen-like material occurs in carbonaceous meteorites (Kerridge et al., 1987) and consists of masses of small-to-large aromatic moieties connected by short aliphatic bridging units. Material with the same composition (carbon, hydrogen, oxygen, nitrogen) and this basic structure also occurs in interstellar dust grains, and is well illustrated by Pendleton and Allamandola (2002, their Fig. 17). Some components of the kerogen-like material can also contribute to the spectral absorption band at 3.3 μm attributed to the C–H aromatic band, as well as the bands near 3.4 μm attributed to C–H stretching in aliphatic hydrocarbons.

In her review of the original draft of this paper, Dr. L.V. Moroz noted that the presence of the 3.29-μm aromatic band suggests that the peripheral aromatic units in the macromolecular structures are not highly substituted, which is in turn consistent with a moderate degree of thermal evolution (but not complete carbonization) of the material. In terms of thermal processing, such an interpretation places the Iapetus and Phoebe material between the highly substituted aromatic-rich organics in CI/CM carbonaceous meteorites and the highly metamorphosed carbonaceous material from the CV/CO chondrites.

Another material of low albedo and red color is the polymer of HCN (Khare et al., 1994). Buratti et al. (2005) used HCN polymer in their models of the reflectance of Iapetus from earlier VIMS data throughout the range 1–5 μm. Materials containing CN are suspected as the cause of the otherwise unidentified 2.41 μm band in the low-albedo material of Iapetus and Phoebe (Clark et al., 2005a, 2005b; Brown et al., 2006), and possibly some of the indistinct spectral structure in the region 4.55–4.8 μm.

We noted above that Owen et al. (2001) proposed that the very strong, broad absorption band centered at 3.0 μm on Iapetus arises from N–H in nitrogen-rich tholin in the surface material. They recognized that O–H is coincident with this band and that H_2O ice on the hemisphere of Iapetus visible from Earth is a contributor to the overall band strength and shape. Owen et al. (2001) reasoned that H_2O is a weak contributor, and an N–H bearing material is abundant because of the rise in the reflectance of the surface longward of about 3.2 μm. Indeed, H_2O ice bands at 1.5 and 2.0 μm, although relatively weak, are clearly present in the Earth-based spectra. However, in the VIMS Iapetus spectrum selected to emphasize the organic bands, the 1.5- and 2.0-μm H_2O ice bands are very weak. From this observation we conclude that the O–H contribution to the 3.0-μm band in Fig. 1 is relatively small, but not negligible. The complete modeling of this region of the spectrum and a determination of the role of tholins will be the subject of a separate investigation.

Many other complex organic molecules occur in meteorites, interplanetary dust particles, and captured comet dust that can be examined in the laboratory, some of which appears to be related to origins in interstellar space by the enhancement of deuterium relative to the solar value. The remote detection of specific classes of organic compounds in the low-albedo surface materials common to many Solar System bodies has proven to be difficult, and in all but a few cases, inconclusive. The difficulties arise because of the low reflectance of the material, the intrinsic weakness of the spectral features in the available wavelength regions, strong dilution by opaque and spectrally featureless species, and other factors. In the interstellar medium the signatures of aromatic and aliphatic molecules can be seen in absorption when background starlight traverses many lightyears through a molecular cloud, and even then the spectral bands are quite weak. In contrast, the small fraction of the sunlight incident on a low-albedo planetary surface that is scattered back into space may penetrate a few micrometers into the surface, but it will not traverse many particles and will consequently fail to acquire the diagnostic spectral signatures of the materials of that surface. Instead, the scattered sunlight can show a new spectral energy distribution, or color, and it is often the color that suggests the presence of organic materials that are not oth-

erwise revealed by discrete and diagnostic spectral bands (e.g., Cruikshank et al., 2005).

The detection of discrete spectral features attributed to polycyclic aromatic hydrocarbons reported in this paper help strengthen the view that refractory organic materials are a significant component of planetary bodies and are indeed responsible for the color properties of at least some of these objects (Cruikshank et al., 2005), although the origins of this material remain to be illuminated.

Acknowledgments

We thank Drs. L.J. Allamandola, M.P. Bernstein, Andrew Mattioda, B.N. Khare, and Allan Meyer for valuable discussions during the preparation of this paper. In her role as a referee, Dr. L.V. Moroz provided valuable comments, clarifications, and insights into the data interpretation, for which we are grateful.

References

Bernard, J.-M., Quirico, E., Brissaud, O., Montagnac, G., Reynard, B., McMillan, P., Coll, P., Nguyen, M.-J., Raulin, F., Schmitt, B., 2006. Reflectance spectra and chemical structure of Titan's tholins: Application to the analysis of Cassini–Huygens observations. Icarus 185, 301–307.

Bernatowicz, T.J., Cowsik, R., Gibbons, P.C., Lodders, K., Fegley Jr., B., Amari, S., Lewis, R.S., 1996. Constraints on stellar grain formation from presolar graphite in the Murchison meteorite. Astrophys. J. 472, 769–782.

Bernstein, M.P., Sandford, S.A., Allamandola, L.J., 1996. Hydrogenated polycyclic aromatic hydrocarbons and the 2940 and 2850 wavenumber (3.40 and 3.51 micron) infrared emission features. Astrophys. J. 472, L127–L130.

Bernstein, M.P., Sandford, S.A., Allamandola, L.J., 2005. The mid-infrared absorption spectra of neutral polycyclic aromatic hydrocarbons in conditions relevant to dense interstellar clouds. Astrophys. J. Suppl. 161, 53–64.

Brown, R.H., Baines, K.H., Bellucci, G., Bibring, J.-P., Buratti, B.J., Bussoletti, E., Capaccioni, F., Cerroni, P., Clark, R.N., Coradini, A., Cruikshank, D.P., Drossart, P., Formisano, V., Jaumann, J., Langevin, Y., Matson, D.L., McCord, T.B., Mennella, V., Miller, E., Nelson, R.M., Nicholson, P.C., Sicardy, B., Sotin, C., 2004. The Cassini Visual and Infrared Mapping Spectrometer investigation. Space Sci. Rev. 115, 111–168 (Cassini Issue).

Brown, R.H., Baines, K.H., Bellucci, G., Buratti, B.J., Capaccioni, F., Cerroni, P., Clark, R.N., Coradini, A., Cruikshank, D.P., Drossart, P., Formisano, V., Jauman, R., Langevin, Y., Matson, D.L., McCord, T.B., Mennella, V., Nelson, R.M., Nicholson, P.D., Sicardy, B., Sotin, C., Baugh, N., Griffith, C.A., Hansen, G.B., Hibbitts, C.A., Momary, T.W., Showalter, M.R., 2006. Observations in the Saturn system during approach and orbital insertion, with Cassini's Visual and Infrared Mapping Spectrometer (VIMS) 2006. Astron. Astrophys. 446, 707–716.

Buratti, B.J., and the VIMS Team, 2005. *Cassini* Visual and Infrared Mapping Spectrometer observations of Iapetus: Detection of CO_2. Astrophys. J. 622, L149–L152.

Cassini, G.D., 1672. Phil. Trans. 12, 831; quoted in Alexander, A.F.O'D., 1962. The Planet Saturn. McMillan, New York, 474 pp.

Chaban, G.M., Bernstein, M., Cruikshank, D.P., 2007. Carbon dioxide on planetary bodies: Theoretical and experimental studies of molecular complexes. Icarus 187, 592–599.

Clark, R.N., Brown, R., Baines, K., Bellucci, G., Bibring, J., Buratti, B., Capaccioni, F., Cerroni, P., Combes, M., Coradini, A., Cruikshank, D., Drossart, P., Filacchione, G., Formisano, V., Jaumann, R., Langevin, Y., Matson, D., McCord, T., Mennella, V., Nelson, R., Nicholson, P., Sicardy, B., Sotin, C., Curchin, J., Hoefen, T., 2005a. Cyanide compositional mapping of surfaces in the Saturn system with Cassini VIMS: The role of water, cyanide compounds and carbon dioxide. In: American Geophysical Union, Fall Meeting 2005a. Abstract P22A-02.

Clark, R.N., Brown, R.H., Jaumann, R., Cruikshank, D.P., Nelson, R.M., Buratti, B.J., McCord, T.B., Lunine, J., Hoefen, T.M., Curchin, J.M., Hansen, G., Hibbitts, C., Matz, K.-D., Baines, K., Bellucci, H.G., Bibring, J.-P., Capaccione, F., Cerroni, P., Coradini, A., Formisano, V., Langevin, Y., Matson, D.L., Mennella, V., Nicholson, P.D., Sicardy, B., Sotin, C., 2005b. Compositional mapping of Saturn's moon Phoebe with imaging spectroscopy. Nature 435, 66–69.

Colangeli, L., Mennella, V., Baratta, G.A., Bussoletti, E., Strazzulla, G., 1992. Raman and infrared spectra of polycyclic aromatic hydrocarbon molecules of possible astrophysical interest. Astrophys. J. 396, 369–377.

Coradini, A., Tosi, F., Gavrishin, A.I., Capaccioni, F., Cerroni, P., Filacchione, G., Adriani, A., Brown, R.H., Bellucci, G., Formisano, V., D'Aversa, E., Lunine, J.I., Baines, K.H., Bibring, J.-P., Buratti, B.J., Clark, R.N., Cruikshank, D.P., Combes, M., Drossart, P., Jaumann, R., Langevin, Y., Matson, D.L., McCord, T.B., Mennella, V., Nelson, R.M., Nicholson, P.D., Sicardy, B., Sotin, C., Hedman, M.M., Hansen, G.B., Hibbitts, C.A., Showalter, M., Griffith, C., Strazzulla, G., 2006. Identification of spectral units on Phoebe. Icarus, in press.

Cronin, J.R., Pizzarello, S., Cruikshank, D.P., 1988. Organic matter in carbonaceous chondrites, planetary satellites, asteroids and comets. In: Kerridge, J.F., Matthews, M.S. (Eds.), Meteorites and the Early Solar System. Univ. of Arizona Press, Tucson, pp. 819–857.

Cruikshank, D.P., Bell, J.F., Gaffey, M.J., Brown, R.H., Howell, R., Beerman, C., Rognstad, M., 1983. The dark side of Iapetus. Icarus 53, 90–104.

Cruikshank, D.P., Schmitt, B., Roush, T.L., Owen, T.C., Quirico, E., Geballe, T.R., de Bergh, C., Bartholomew, M.J., Dalle Ore, C.M., Douté, S., Meier, R., 2000. Water ice on Triton. Icarus 147, 309–316.

Cruikshank, D.P., Imanaka, H., Dalle Ore, C.M., 2005. Tholins as coloring agents on outer Solar System bodies. Adv. Space Res. 36, 178–183.

d'Hendecourt, L.B., Allamandola, L.J., 1986. Time dependent chemistry in dense molecular clouds. III. Infrared band cross-sections of molecules in the solid state at 10 K. Astron. Astrophys. Suppl. 64, 453–467.

Douté, S., Schmitt, B., Quirico, E., Owen, T.C., Cruiskhank, D.P., de Bergh, C., Geballe, T.R., Roush, T.L., 1999. Evidence for methane segregation at the surface of Pluto. Icarus 142, 421–444.

Gaffey, M., Lebofsky, L., Nelson, M., Jones, T., 1993. Asteroid surface compositions from Earth-based reflectance spectroscopy. In: Peters, C.M., Englert, P.A.J. (Eds.), Remote Geochemical Analysis; Elemental and Mineralogical Composition. Cambridge Univ. Press, Cambridge, pp. 437–453.

Gudipati, M.S., Dworkin, J., Chillier, X.D.F., Allamandola, L.J., 2003. Luminescence from vacuum-ultraviolet-irradiated cosmic ice analogs and residues. Astrophys. J. 583, 514–523.

Imanaka, H., Khare, B.N., Elsila, J.E., Bakes, E.L.O., McKay, C.P., Cruikshank, D.P., Sugita, S., Matsui, T., Zare, R.N., 2004. Laboratory experiments of Titan tholin formed in cold plasma at various pressures: Implications for nitrogen-containing polycyclic aromatic compounds in Titan haze. Icarus 168, 344–366.

Jourdain de Muizon, M., Geballe, T.R., d'Hendecourt, L.B., Baas, F., 1986. New emission features in the infrared spectra of two *IRAS* sources. Astrophys. J. 306, L105–L108.

Kerridge, J., Chang, S., Shipp, R., 1987. Isotopic characterization of kerogen-like material in the Murchison carbonaceous chondrite. Geochim. Cosmochim. Acta 51, 2527–2540.

Khare, B.N., Sagan, C., Thompson, W.R., Arakawa, E.T., Meisse, C., Tuminello, P.S., 1994. Optical properties of poly-HCN and their astronomical applications. Can. J. Chem. 72, 678–694.

Messenger, S., Amari, S., Gao, X., Walker, R.M., Clemett, S.J., Chillier, X.D.F., Zare, R.N., Lewis, R.S., 1998. Indigenous polycyclic aromatic hydrocarbons in circumstellar graphite grains from primitive meteorites. Astrophys. J. 502, 284–295.

Moroz, L.V., Arnold, G., Korochantsev, A.V., Wäsch, R., 1998. Natural solid bitumens as possible analogs for cometary and asteroid organics. Icarus 134, 253–268.

Murphy, R.E., Cruikshank, D.P., Morrison, D., 1972. Radii, albedos, and 20-micron brightness temperatures of Iapetus and Rhea. Astrophys. J. 177, L93–L96.

Owen, T.C., Cruikshank, D.P., Dalle Ore, C.M., Geballe, T.R., Roush, T.L., de Bergh, C., 1999. Detection of water ice on Saturn's satellite Phoebe. Icarus 139, 379–382.

Owen, T.C., Cruikshank, D.P., Dalle Ore, C.M., Geballe, T.R., Roush, T.L., de Bergh, C., Pendleton, Y.J., Khare, B.N., 2001. Decoding the domino: The dark side of Iapetus. Icarus 149, 160–172.

Pendleton, Y.J., Allamandola, L.J., 2002. The organic refractory material in the diffuse interstellar medium: Mid-infrared spectroscopic constraints. Astrophys. J. Suppl. 138, 75–98.

Pendleton, Y.J., Sandford, S.A., Allamandola, L.J., Tielens, A.G.G.M., Sellgren, K., 1994. Near-infrared absorption spectroscopy of interstellar hydrocarbon grains. Astrophys. J. 437, 683–696.

Porco, C.C., and the Cassini Imaging Team, 2005. Cassini imaging science: Initial results on Phoebe and Iapetus. Science 307, 1237–1242.

Quirico, E., Douté, S., Schmitt, B., de Bergh, C., Cruikshank, D.P., Owen, T.C., Geballe, T.R., Roush, T.L., 1999. Composition, physical state and distribution of ices at the surface of Triton. Icarus 139, 159–178.

Sandford, S.A., Allamandola, L.J., Tielens, A.G.G.M., Sellgren, K., Tapia, M., Pendleton, Y., 1991. The interstellar C–H stretching band near 3.4 microns—Constraints on the composition of organic material in the diffuse interstellar medium. Astrophys. J. 371, 607–620.

Vilas, F., Larson, S.M., Stockstill, K.R., Gaffey, M.J., 1996. Unraveling the zebra: Clues to the Iapetus dark material composition. Icarus 124, 262–267.

Zellner, B., 1972. On the nature of Iapetus. Astrophys. J. 174, L107–L109.